Petrogenetic linkages among Martian basalts: Implications based on trace element chemistry of olivine

C. K. SHEARER[1*], P. V. BURGER[1], J. J. PAPIKE[1], L. E. BORG[2], A. J. IRVING[3], and C. HERD[4]

[1]Institute of Meteoritics, Department of Earth and Planetary Sciences, University of New Mexico,
New Mexico 87131, Albuquerque, USA
[2]Lawrence Livermore National Laboratory, Livermore, California 94551, USA
[3]Department of Earth and Space Sciences, University of Washington, Seattle, Washington 98195, USA
[4]Department of Earth and Atmospheric Sciences, University of Alberta, Edmonton, Alberta, T6G 2E3, Canada
*Corresponding author. E-mail: cshearer@unm.edu

Abstract–The shergottites exhibit a range of major and trace element compositions, crystallization ages, and initial Sr, Nd, Hf, and Pb isotopic compositions. To constrain the physical mechanisms by which shergottites obtain their compositional characteristics, we examined the major and trace element record preserved in olivine in the more primitive shergottites. Based on such characteristics as the Mg#, V zoning, calculated $D_{Ni,Co}$, the olivine in Y-980459 are most likely phenocrysts. Many of these same characteristics indicate that the olivines in other shergottites are not in equilibrium with the adjacent melt. However, in most cases they are not xenocrystic, but additions of olivine from the same basaltic system. Elephant Moraine (EET) A79001 may be an exception with the olivine data suggesting that it is xenocrystic. In this case, the olivine crystallized from a reduced and LREE-depleted melt and was incorporated into an oxidized and enriched basalt. Vanadium and CaO in olivine appear to record the appearance of spinel and pyroxene on the liquidus of most of the shergottites. Most of the olivine shergottites represent basalts produced by melting of reduced (IW to IW + 1), depleted mantle sources. Olivine data indicate that many of the primary melts derived from this source had similar Ni, Co, and Mn. Shergottites such as Northwest Africa (NWA) 1110/1068 and perhaps Roberts Massif (RBT) 04261 that appear to be derived from more enriched sources have distinctly different olivine. In the case of NWA 1110/1068, the olivine data suggests that the enriched component was added to system prior to olivine crystallization.

INTRODUCTION

The shergottites (basaltic and lherzolitic Martian meteorites) exhibit a range of major and trace element compositions, initial Sr, Nd, Hf, and Pb isotopic compositions (Fig. 1), and crystallization ages (Table 1) (e.g., Shih et al. 1982; Blichert Toft et al. 1999; Wadhwa 2001; Borg et al. 2003, 2005; Herd et al. 2002a; Herd 2003; Symes et al. 2008). Variations in isotopic (i.e., ε_{Nd} – $^{87}Sr/^{86}Sr$) and trace element compositions (i.e., REE) define a wide continuum (Fig. 1) among the shergottites from those which are highly incompatible element depleted to those that are incompatible element enriched. Associated with these variations in geochemical parameters are variations in fO_2 conditions under which the shergottites crystallized (2 to 4 log units; Wadhwa 2001; Herd et al. 2002a, 2002b; Goodrich et al.

2003; Herd 2003). These correlations have been interpreted as indicating the presence of reduced, incompatible element-depleted and oxidized, incompatible element-enriched reservoirs that were produced during early stages of Martian differentiation (≈4.5 Ga) (Wadhwa 2001; Herd et al. 2002a; Borg et al. 2003; Goodrich et al. 2003; Herd 2003; Jones 2003; Symes et al. 2008). Martian basaltic magmatism represented by the shergottites is thought to represent mixing between these two reservoirs. Symes et al. (2007) demonstrated that this mixing could not be a product of simple assimilation between a single mantle-derived basalt and a single crustal reservoir. Whether this mixing process is a product of more complex assimilation processes between the Martian crust and a series of mantle-derived magmas or mixing of distinctly different mantle reservoirs during melting is still a point of debate (Shih et al. 1993; Borg et al.
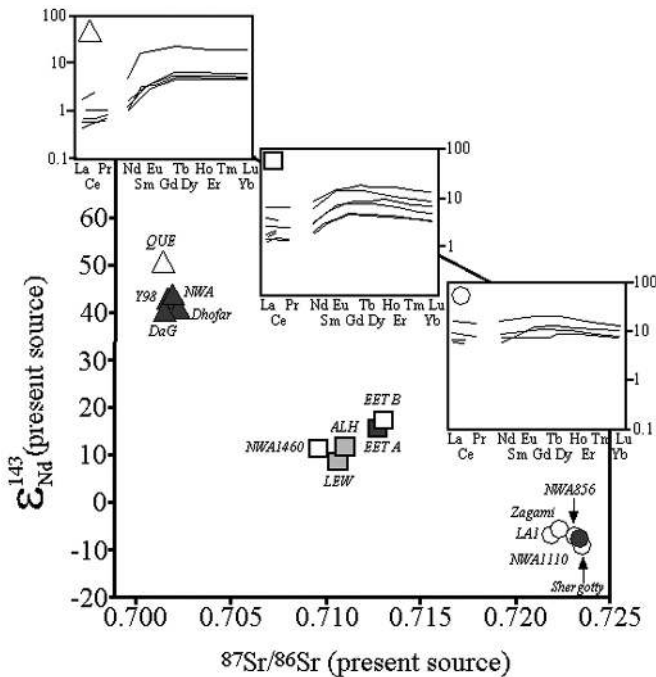
Fig. 1. Plot of ε_{Nd}^{143} (present source) versus Sr^{87}/Sr^{86} (present source) for shergottites. Inserted are REE patterns for each designated group (triangles, squares, circles). Gray symbols represent lherzolitic shergottites. Black symbols represent olivine-bearing shergottites. Open symbols represent shergottites dominated by a mineralogy of pyroxene + plagioclase. Modified after Borg (2007) and Symes et al. (2007).

1997; Wadhwa 2001; Herd et al. 2002a; Goodrich et al. 2003; Herd 2003; Jones 2003; Symes et al. 2008).

The goal of this study is to provide additional constrains on the physical mechanisms by which shergottites obtain their compositional characteristics. This new perspective is accomplished through a major and trace element study of one of the earliest crystallizing phases in some of the more primitive shergottites. Here, we define the petrogenesis of olivine megacrysts in the olivine-bearing shergottites, evaluate its use in recording the earliest stages of Martian basalt crystallization, compare olivine major and trace element characteristics among the shergottites, compare olivine in olivine-bearing Martian basalts to olivine in other Martian basaltic lithologies (lherzolitic shergottites, nahklites) and discuss the relevance of this data to interpreting the Martian surface as determined by the Mars Exploration Rover (MER) mission.

OLIVINE-BEARING SHERGOTTITES

At least 40 unpaired meteorites have been acknowledged as samples derived from Mars (Meyer 2007). All of them have an igneous origin and formed by the crystallization of basaltic magmas on or near the Martian surface. This suite of Martian meteorites comprise five major rock types including

an orthopyroxenite, clinopyroxenites, dunites, lherzolitic basalts and basalts (e.g., McSween 1994; McSween and Treiman 1999). The lherzolitic basalts are referred to in the meteorite literature as lherzolitic shergottites. The basalts have been divided into three subclasses: olivine-phyric, olivine-orthopyroxene-phyric, and basaltic shergottites. In the remainder of the paper, we refer to the Martian basalts that contain early olivine (versus late-stage fayalite) as olivine-bearing shergottites. Olivine-bearing shergottites analyzed in this study are: Yamato (Y-) 980459, Northwest Africa (NWA) 2626, NWA 2046, NWA 1195, NWA 1110/1068, Dhofar 019, Sayh al Uhaymir (SaU) 005, Elephant Moraine (EET) A79001 lithology A, Dar al Gani (DaG) 476, and Roberts Massif (RBT) 04261. These ten olivine-bearing shergottites have been previously studied in a variety of detail (e.g., Irving et al. 2002; Goodrich et al. 2003; Herd 2003; McKay et al. 2004; Edmunson et al. 2005). Detailed descriptions of individual Martian meteorites and comprehensive summaries of previous studies are presented in the Mars Meteorite Compendium (Meyer 2007; updates at http://curator.jsc.nasa.gov/antmet/ mmc/ mmc.htm). Where the data is available, the ε_{Nd} − $^{87}Sr/^{86}Sr$ characteristics of the olivine-bearing basalts cover the entire range exhibited by the shergottites (Fig. 1). However, a majority appear to be associated with the most depleted shergottites. For the purpose of comparison, we also analyzed olivine from other olivine-bearing lithologies in Martian meteorites: lherzolitic shergottites (Lewis Cliff [LEW] 88516, Allan Hills [ALH] 77005) and clinopyroxenites (Governador Valadares, Miller Range [MIL] 03346).

The olivine-bearing shergottites consist of olivine megacrysts (or phenocrysts or xenocrysts) in a basaltic matrix (Fig. 2). The modal abundance of olivine megacrysts in the shergottites studied varies considerably from 3 to 26%. The modal abundance of olivine in the lherzolitic shergottites and clinopyroxenites ranges from 22–60% and 2–20%, respectively. The textural relationship between the large olivine megacrysts and the associated basaltic matrix has been a point of dispute and several petrogenetic models have been suggested to explain the origin of this texture. They include: lithologies representing a basaltic melt composition which contain phenocrystic olivine in equilibrium with that melt, lithologies representing a basaltic melt plus minor accumulation of additional phenocrystic olivine, lithologies representing a basaltic melt plus accumulation of megacrystic olivine from the same overall system (i.e., "cogenetic"), and lithologies representing xenocrystic olivine that was randomly incorporated into a basaltic melt that was derived either through mantle or impact melting (McSween and Jarosewich 1983; Wadhwa et al. 1994; Treiman 1995; McSween and Treiman 1998; Mittlefehldt et al. 1999; Barrat et al. 2002; Herd et al. 2002b; Irving et al. 2002, 2005; Wadhwa and Crozaz, 2002; Koizumi et al. 2004; McKay et al. 2004; Shearer et al. 2006). These are the

Table 1. Shergottites used in this study with their crystallization ages and presents/absence of olivine in groundmass.

Shergottite	Crystallization age	% olivine	Olivine in groundmass
EETA79001 A	173 ± 10 Ma [1] Rb-Sr	7–10, Fo_{81-55}	No
NWA 1110/1068	185 ± 11 Ma [2] Sm-Nd	21–27, Fo_{70-50}	No
Y-980459	472 ± 47 Ma [3] Sm-Nd	9–26, Fo_{86-32}	Yes
SaU 005/094		22–31, Fo_{72-65}	Yes
Dhofar 019	575 ± 7 Ma [4] Sm-Nd	9–14, Fo_{75-25}	Yes
DaG 476/489	474 ± 11 Ma [5] Sm-Nd	10–24, Fo_{76-58}	No
NWA 2626		15%, Fo_{83-53}	Yes
NWA 2046		17%, Fo_{84-42}	Yes
NWA 1195		22%, Fo_{81-60}	No
RBT 04261		12%, Fo_{70-58}	NA

[1] Wooden et al. (1982). [2] Shih et al. (2003), [3] Shih et al. (2005). [4] Borg et al. (2001). [5] Borg et al. (2000).
NA: Texture is significantly different from many of the other olivine-bearing shergottites that distinction between olivine megacrysts and olivine in groundmass is less significant.

Table 2. Selected major and trace element analyses of olivine from shergottites and nahklites. Formula for olivine analyses are calculated based on 4 oxygen.

Sample	RBT	RBT	EETA	EETA	EETA	Y98	Y98	Y98	NWA 1110	NWA 1110	NWA 1110
Point #	48	135	39	101	51	r-6	c-11	i-3	T3-5	T5-16	T2-5
SiO_2	36.59	36.7	35.75	38.73	37.45	39.38	38.78	38.23	34.75	38.96	35.61
TiO_2	0.01	0.02	0.02	0.00	0.01	0.00	0.01	0.02	0.01	0.00	0.00
Cr_2O_3	0.01	0.02	0.03	0.00	0.04	0.31	0.2	0.16	0.00	0.05	0.039
FeO	33.97	31.89	35.42	20.46	27.29	14.36	19.15	23.17	41.7	23.01	36.45
MgO	28.02	30.86	27.41	40.22	34.47	44.42	40.59	37.6	21.61	37.1	26.87
MnO	0.66	0.64	0.68	0.43	0.53	0.35	0.42	0.58	0.8	0.46	0.74
CaO	0.27	0.19	0.24	0.05	0.23	0.18	0.23	0.37	0.29	0.24	0.17
Total	99.53	100.32	99.55	99.89	100.02	99.00	99.38	100.13	99.16	99.82	99.879
T-site											
Si	1.015	0.999	1.001	1.000	1.000	0.999	1.001	1.000	1.010	1.017	0.999
Ti	0.000	0.001	0.001	0.000	0.001	0.000	0.000	0.000	0.000	0.000	0.000
Total	1.015	1.000	1.002	1.000	1.001	0.999	1.001	1.000	1.010	1.017	0.999
O-site											
Cr	0.000	0.000	0.001	0.000	0.001	0.006	0.004	0.003	0.000	0.001	0.001
Fe	0.788	0.726	0.829	0.442	0.609	0.304	0.414	0.507	1.014	0.503	0.885
Mg	1.158	1.252	1.144	1.548	1.371	1.676	1.562	1.465	0.937	1.444	1.123
Mn	0.016	0.015	0.016	0.009	0.012	0.008	0.009	0.012	0.02	0.01	0.017
Ca	0.008	0.006	0.007	0.001	0.006	0.005	0.006	0.01	0.009	0.007	0.005
Total	1.970	1.999	1.997	2.000	1.999	1.998	1.995	1.998	1.979	1.965	2.002
Mg#	0.59	0.63	0.58	0.78	0.69	0.85	0.79	0.74	0.48	0.74	0.57
Trace elements (ppm)											
Sc	20	20	10	13.1	9	16.7	10.8	12.3	18.8	19.1	18.1
Ni	1379	1495	550	1120	1014	997	1448	1326	1070	1447	1330
Co	245	250	230	185	170	155	124	112	270	201	225
V	10	9	14	28	23	39.7	33.4	33.8	9.1	14.8	12.5
Ti	214	144	145	120	91	63	98	61	195	129	129
Y	1.1	0.8	0.24	0.09	0.16	0.22	0.17	0.22	1.5	1	1.2

Sample	NWA 2626	NWA2626	NWA2626	SAU 005	SAU 005	SAU 005	NWA 1195	NWA 1195	NWA 1195	NWA 2046	NWA 2046
point #	T2-11	T1-1	T2-5	3-020	3-122	3-5	1247	C-11	1259	T1-7	T1-25
SiO_2	38.97	36.25	37.11	36.96	37.99	37.29	35.7	38.88	37.02	39.08	35.37
TiO_2	0.01	0.03	0.01	0.01	0.00	0.01	0.02	0.01	0.00	0.00	0.03
Cr_2O_3	0.12	0.02	0.04	0.03	0.05	0.03	0.06	0.08	0.00	0.08	0.10
FeO	17.86	33.74	28.23	29.45	23.48	26.74	36.85	19.27	32.51	18.80	38.08
MgO	41.55	28.85	33.05	32.18	37.36	34.47	27.05	41.09	30.44	42.21	25.9
MnO	0.37	0.67	0.52	0.59	0.52	0.48	0.66	0.40	0.61	0.38	0.72

Table 2. *(Continued).* Selected major and trace element analyses of olivine from shergottites and nahklites. Formula for olivine analyses are calculated based on 4 oxygen.

Sample	RBT	RBT	EETA	EETA	EETA	Y98	Y98	Y98	NWA 1110	NWA 1110	NWA 1110
CaO	0.13	0.24	0.18	0.3	0.21	0.36	0.39	0.27	0.25	0.24	0.21
Total	99.01	9.8	99.14	99.52	199.61	99.38	100.73	100.00	100.83	100.79	100.41
T-site											
Si	1.003	1.003	1.004	1.001	1.000	1.001	0.994	0.998	1.005	0.997	0.995
Ti	0.000	0.001	0.000	0.000	0.000	0.000	0.000	0.000	0.000	0.000	0.001
Total	1.003	1.004	1.004	1.001	1.000	1.000	0.994	0.998	1.005	0.997	0.996
O-site											
Cr	0.003	0.000	0.001	0.005	0.001	0.001	0.001	0.002	0.000	0.002	0.002
Fe	0.384	0.781	0.639	0.667	0.517	0.600	0.858	0.414	0.738	0.397	0.896
Mg	1.594	1.189	1.333	1.300	1.465	1.375	1.123	1.572	1.231	1.589	1.086
Mn	0.008	0.016	0.012	0.014	0.011	0.011	0.016	0.009	0.014	0.008	0.017
Ca	0.004	0.007	0.005	0.009	0.006	0.010	0.012	0.007	0.007	0.006	0.006
Total	1.993	1.993	1.990	1.995	2.000	1.998	2.010	2.003	1.991	2.002	2.006
Mg#	0.81	0.60	0.68	0.66	0.74	0.70	0.57	0.790	0.630	0.80	0.55
Trace elements (ppm)											
Sc	17	11.5	14.7	14.3	13	12.6	18.6	15.1	14.0	16.7	9.2
Ni	748	1326	1057	817	1142	1003	606	1210	827	706	1240
Co	202	112	168	231	208	214	253	190	250	230	160
V	9	33.5	12.3	23.1	24.5	20.2	12.5	22.1	14.6	10.6	17.4
Ti	235	104	205	119	83.3	103	226	264	198	139	114
Y	0.37	0.22	0.43	0.51	0.25	0.3	0.7	0.28	0.44	0.41	0.32

| Sample	NWA 2046	DaG	DaG	LEW	LEW	ALH	ALH	GOV-VAL	GOV-VAL	MIL	MIL
Point#	T1-13	24-1	23-3	F/G	L	IP3	A	14-3	9-2	16-11	20-05
SiO_2	38.4	38.34	36.14	37.55	36.72	37.47	38.35	32.26	33.50	34.25	34.08
TiO_2	0.03	0.00	0.00	0.02	0.03	0.04	0.02	0.02	0.02	0.01	0.02
Cr_2O_3	0.13	0.06	0.04	0.1	0.03	0.04	0.05	0.01	0.11	0.01	0.01
FeO	24.32	20.49	32.18	26.14	32.12	28.05	37.68	58.45	49.99	46.83	45.93
MgO	37.23	38.15	29.32	34.84	30.93	34.74	24.07	9.44	14.70	17.79	19.00
MnO	0.5	0.01	0.02	0.28	0.08	0.23	0.05	0.88	0.65	1.09	0.98
CaO	0.23	0.3	0.27	0.14	0.15	0.03	0.16	0.29	0.4	0.38	0.46
Total	100.84	97.35	97.97	99.07	100.06	100.6	100.38	101.35	99.37	100.37	100.48
T-site											
Si	1.000	1.015	1.009	1.005	1.001	0.996	1.001	1.004	1.016	1.011	1.000
Ti	0.001	0.000	0.000	0.000	0.001	0.001	0.000	0.000	0.000	0.000	0.000
Total	1.001	1.015	1.009	1.005	1.002	0.997	1.001	1.004	1.016	1.001	1.000
O-site											
Cr	0.003	0.001	0.001	0.002	0.001	0.001	0.001	0.000	0.003	0.000	0.000
Fe	0.530	0.454	0.752	0.585	0.732	0.623	0.525	1.521	1.268	1.156	1.128
Mg	1.446	1.505	1.220	1.390	1.257	1.376	1.465	0.438	0.665	0.783	0.831
Mn	0.011	0.000	0.000	0.006	0.002	0.005	0.001	0.023	0.017	0.027	0.024
Ca	0.006	0.009	0.008	0.004	0.004	0.001	0.004	0.010	0.013	0.012	0.014
Total	1.996	1.969	1.981	1.988	1.996	2.006	1.996	1.992	1.966	1.978	1.999
Mg#	0.73	0.77	0.62	0.70	0.63	0.69	0.74	0.22	0.34	0.4	0.420
Trace elements (ppm)											
Sc	12.7	13.7	18.1	10.9	10.9	13	8.7	14.4	23.1	21.4	15
Ni	1078	900	598	943	624	691	926	556	819	434	797
Co	195	198	227	190	197	195	107	332	361	382	358
V	23.5	41.9	31	30	15.3	7	11	3.7	4.6	16.1	9.9
Ti	69	96	157	130	188	195	107	290	157	360	193
Y	0.42	0.38	0.56	0.4	0.12	0.15	0.13	0.69	0.59	0.74	0.44
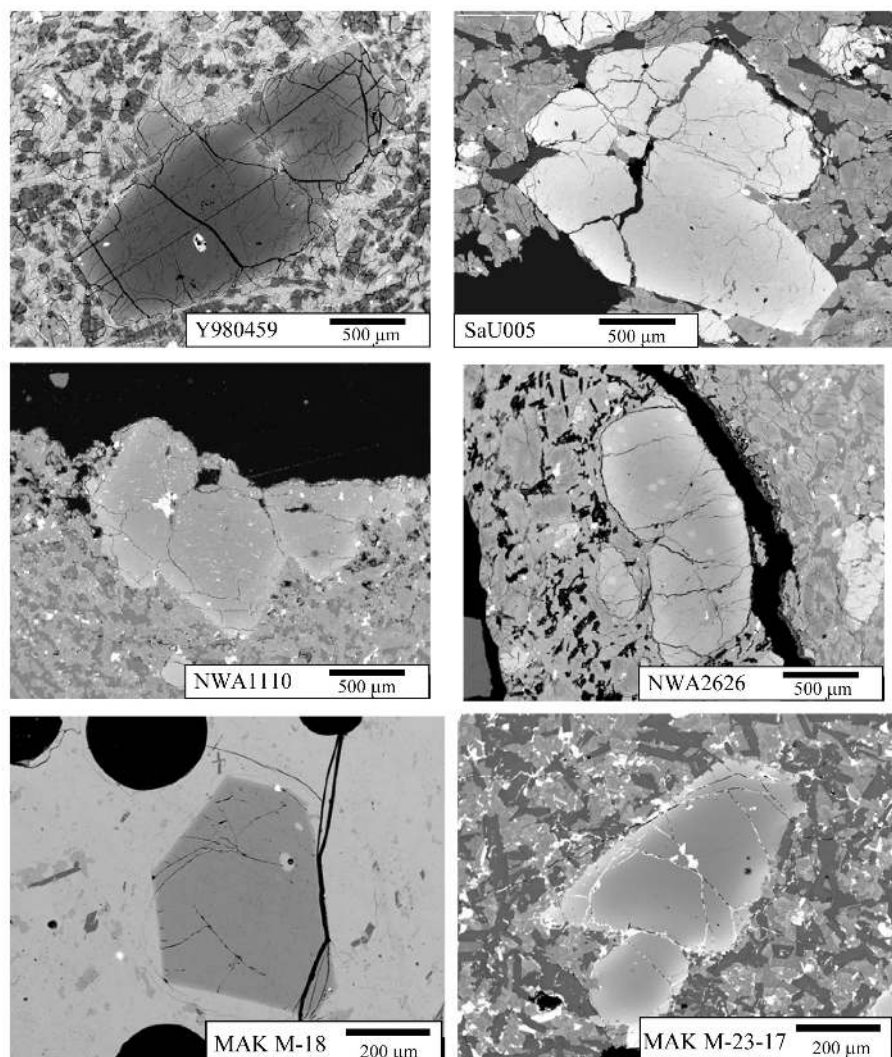
Fig. 2. BSE images of Y-980459, SaU 005, NWA 1110/1068, and NWA 2626 illustrating the textural variations exhibited by the olivine-phyric shergottites. Included for comparison are two BSE images of olivine from the Makaopuhi lava lake (MAK M-18, MAK M-23-17). Y-980459 is a basalt that exhibits a porphyritic texture defined by olivine megacrysts (16–26%) and medium-grained pyroxenes (48–63%) immersed in mesostasis (25–30%). Plagioclase is absent. SaU 005 exhibits a porphyritic texture defined by large, subhedral and euhedral olivine megacrysts (25%) immersed in a medium-grained groundmass of pyroxene (P) (60%) and maskelynite (10%). The texture in NWA 1110/1068 is defined by subhedral to anhedral olivine megacrysts (21–27) immersed in a fine-grained groundmass of pyroxene (52%) and shocked plagioclase (15–22%). The texture in NWA 2626 is defined by subhedral to anhedral olivine megacrysts and elongate phenocrysts of orthopyroxene immersed in a mesostasis of intergrown pyroxene and shocked plagioclase. The Makaopuhi lava lake was a formed during the eruption of the Kilauea volcano March 5–15, 1965 and is considered to be a closed, basaltic system (Hagerty et al. 2006 and references within). Sample MAK M-18 was collected on March 14, 1965 from the surface of the Makaopuhi lava lake at a temperature of 1160 °C and consists of 5.5% euhedral olivine phenocrysts and 86% glass (with minor augite and plagioclase). Sample MAK M-23-17 was collected on November 9, 1965 from a depth of approximately 5.5 m and at a temperature of 990–1005 °C. It consists of 2% partially reabsorbed olivine phenocrysts with an iron rich rim and 15% glass (with augite and plagioclase). Clearly, reabsorbed textures as exhibited by the olivine in many of the olivine-bearing shergottites do not necessarily mean that these megacrysts are xenocrystic.

overall definitions that we will attach to phenocrysts, megacrysts, and xenocrysts in this manuscript. The appearance of early olivine in these basalts and their relatively high bulk Mg# relative to basaltic shergottites make them one of the earliest preserved recorders of the geochemical characteristics of primary Martian basaltic magmas. Of these Martian basalts, it has been suggested that Y-980459 most closely approximates a liquid composition and thus provides the clearest vision of the Martian mantle and basaltic processes (Koizumi et al. 2004; McKay et al. 2004; Burgess et al. 2006; Draper 2007).

EXPERIMENTAL DESIGN AND ANALYTICAL APPROACH

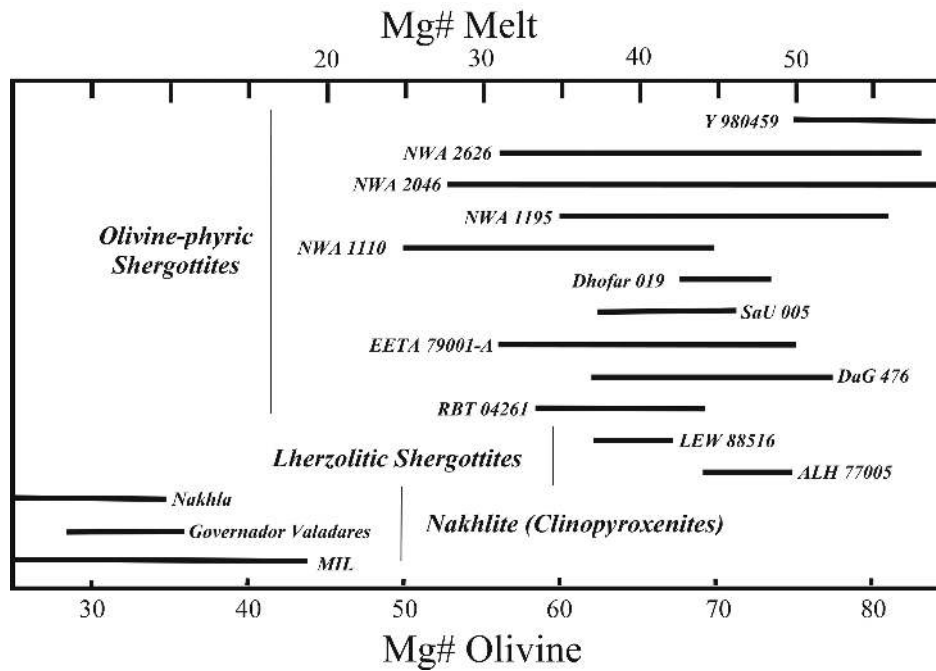Olivine-bearing shergottites (Y-980459, NWA 2626,

Fig. 3. Range in the Mg/(Mg + Fe) of olivine in the meteorites used in this study and calculated melt compositions in equilibrium with the olivine.
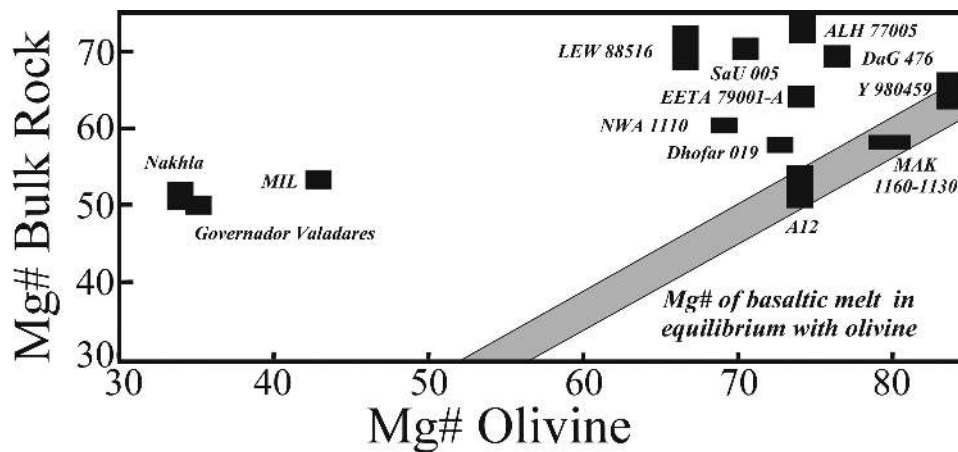

Fig. 4. Plot of Mg/(Mg + Fe) in cores of olivine versus Mg/(Mg + Fe) of bulk rock. Olivine from the Makaopuhi lava lake (MAK) and Apollo 12 olivine basalts are also plotted on the diagram.

NWA 2046, NWA 1195, NWA 1110/1068, Dhofar 019, SaU 005, EETA79001A, DaG 476), lherzolitic shergottites (LEW 88516, ALH 77005, perhaps RBT 04261) and nahklites (Governador Valadares, MIL 03346) were analyzed in this study. Nahklites are thought to represent crystallization products of basaltic melts that are not directly unrelated to the shergottites (i.e., Jones 1989, 2003; McSween and Treiman 1998). Unlike the shergottites, olivine in the nahklites is not an early liquidus phase. The comparisons between the olivine in the shergottites and the nahklites are meant to illustrate the similarities-differences of olivine from these different lithologies. In addition to the products of Martian basaltic

magmatism, we also analyzed two basalts from basaltic systems that crystallized under well defined fO_2: an Apollo 12 olivine basalt 12009, that crystallized at an fO_2 of approximately IW − 1 and a terrestrial basalt from the Makaopuhi lava lake in Hawaii that crystallized at 1145 °C and an fO_2 of IW + 3.65 (= FMQ + 0.15) (Sato and Wright 1966). These samples were selected for comparison to the shergottites because of their well documented conditions of crystallization (well-known fO_2 and temperature), the bulk rock compositions represent melt compositions, the olivine is in equilibrium with the bulk rock composition in numerous samples, and olivine exhibits a range of textural relations with the surrounding
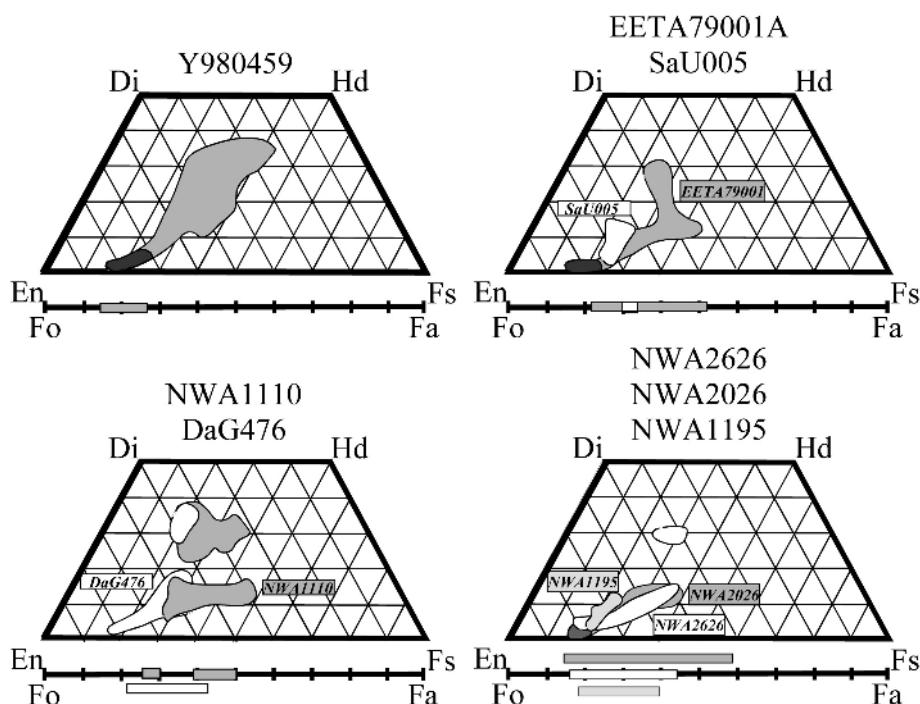
Fig. 5. Summary of the compositional relationships between olivine and pyroxene in the olivine-bearing shergottites.

basaltic melt. Throughout the text, we use this data to make important comparisons with data where it is available.

Olivine in these basalts was first imaged and mapped using a scanning electron microscope (SEM), followed by major element analysis using a JEOL JXA-8200 electron microprobe. A suite of trace elements was analyzed (Sc, V, Ti, Co, Ni, and Y) using a Cameca 4f IMS ion microprobe and previously documented analytical approaches (Shearer et al. 2005). The precision of the analysis of Ni, Co, Ti, and V in the olivine is better than 6%. The precision of the analysis of Sc is better than 10% at concentrations of 10 ppm or higher. The precision of Y is better than 15%. The rationale for analyzing Y in olivine ($D_{olivine} \sim 0.01$) rather than Sm ($D_{olivine} \leq 0.01$) is that its higher abundance in olivine results in better analytical precision. When possible, melt inclusions or embayments in olivine (NWA 1110/1068 and Y-980459) were first imaged by backscattered electrons (EMP) and ions (ion microprobe) and then analyzed for REE. The analytical precision of REE in these melt inclusions is better than 15%. All instruments used in these analyses are housed in the Institute of Meteoritics at the University of New Mexico.

RESULTS

Textural Characteristics of Olivine

Olivine has a wide range of morphologies and textural relationships with adjacent mineral phases. In the olivine-bearing shergottites, the large olivine "megacrysts" commonly occur in

clusters and range in morphology from euhedral (i.e., Y-980459) to corroded/resorbed with thin Fe-rich rims (i.e., NWA 1110/1068) (Fig. 2). In cases in which the olivine is euhedral, the inner and more Mg-rich core will commonly have an anhedral outline that is suggestive of resorption (SaU 005 in Fig. 2). In several samples, euhedral and anhedral olivine may be spatially associated within the same sample (SaU 005 in Fig. 2). These texturally different olivines in SaU 005 have identical major and minor element chemistries. The texture exhibited by RBT 04261 is significantly different from that of the other olivine-phyric shergottites. Rather than being immersed in a finer-grained matrix, the olivine megacrysts are surrounded by rather coarse-grained pyroxene. This is more similar to the textures documented in the lherzolitic shergottite. In Y-980459, the olivine megacrysts are immersed in a groundmass that contains olivine. The occurrence of olivine in the groundmass is common in only half of the olivine-bearing shergottites (Table 1).

Many of the olivine textures observed in the olivine-phyric shergottites are also observed in the closed-basaltic system represented by the Makaopuhi lava lake (Fig. 2). In the Makaopuhi lava lake, early olivine phenocrysts are euhedral and in near equilibrium with adjacent basaltic melt based on Fe-Mg K_D. Finer-grained olivine will occur in the groundmass. In other portions of the lava lake, olivine appears have reacted with the adjacent basalt to form anhedral olivine. The distribution of Fe-Mg between these olivines and the adjacent basalt indicates that the olivine is not in equilibrium with the basalt. Also, in these samples, olivine does not occur in the groundmass. Wright and Okamura (1977) documented
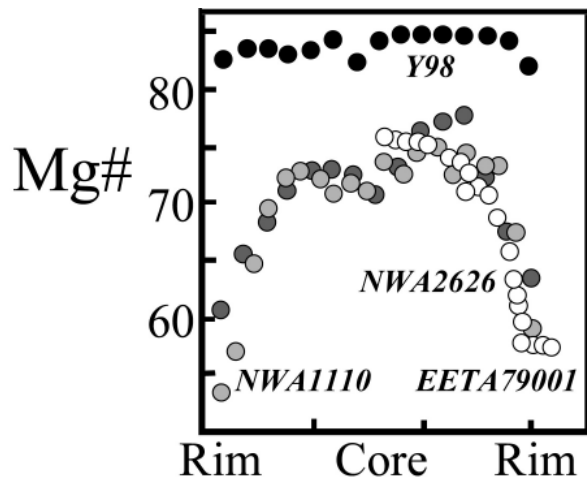
Fig. 6. Zoning of Mg/(Mg + Fe) in olivine from selected olivine-phyric shergottites. Shergottites are represented by the following symbols: Y-980459 = black, EETA79001 = white, NWA 1110/1068 = light gray, and NWA 2626 = dark gray.
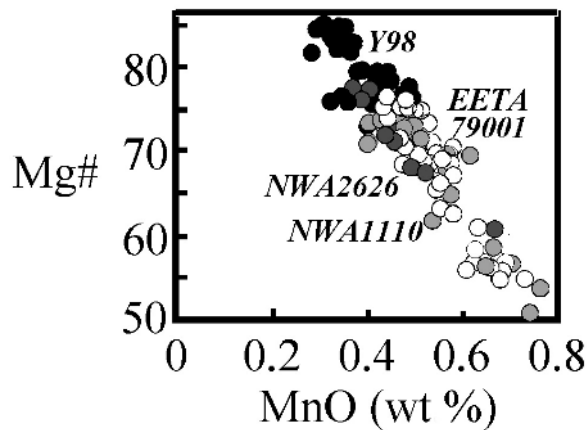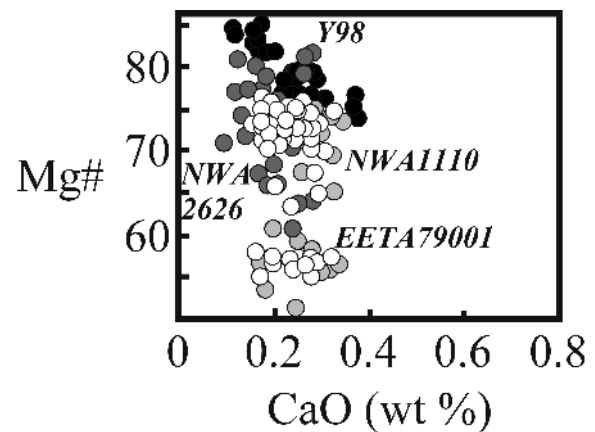

Fig. 7. Zoning of Mg/(Mg + Fe) and MnO in olivine from selected olivine-bearing shergottites. Symbols the same as in Fig. 6.

the role of gravitational settling and convective flow to produce the array of olivine textures observed in this closed-magmatic system.

The textures defined by the megacrysts in the olivine-bearing shergottites significantly contrast with the olivine in the lherzolitic shergottites and nahklites (see summaries in Harvey et al. 1993; McSween and Treiman 1998; Meyer 2007). In the lherzolitic shergottites, the olivine is either independent euhedral-subhedral grains or is anhedral and poikilitically enclosed in pyroxene. In the nahklites, olivine ranges from subhedral grains to post-cumulus infillings among euhedral high-Ca clinopyroxene. The olivine contains inclusions of augite, magnetite, and trapped melt.

Major and Minor Elements in Olivine

The Mg# of the olivine megacrysts in the olivine-bearing shergottites ranges from 85 to 50 (Fig. 3). The olivine cores of

Fig. 8. Zoning of Mg/(Mg + Fe) and CaO in olivine from selected olivine-phyric shergottites. Symbols the same as in Fig. 6.

Y-98045 and NWA 2046 have the highest Mg#. The range of the Mg# of olivine megacrysts observed in the shergottites overlaps with the olivine in the lherzolitic shergottites, but is significantly higher than the nahklites (Mg# = 45 to <25). Based on Fe-Mg exchange K_D between olivine-basalt and experimental studies (i.e., Roeder and Emslie 1970; McKay et al. 2004; Shearer et al. 2006) most of the olivine in the olivine-bearing shergottites are not in equilibrium with the bulk rock compositions with the possible exception of Y-980459 (Fig. 4). This has been documented in many previous studies (i.e., McSween and Jarosewich 1983; Wadhwa et al. 1994; Treiman 1995; McSween and Treiman 1998; Mittlefehldt et al. 1999; Barrat et al. 2002; Herd et al. 2002b; Irving et al. 2002, 2005; Wadhwa and Crozaz 2002; McKay et al. 2004). In comparison, the early olivine from the Makaopuhi lava lake and Apollo 12 olivine basalt (12009) are in equilibrium with the bulk rock and fit within the equilibrium field in Fig. 4.

The compositional relationships between olivine and pyroxene within each olivine-bearing shergottite analyzed in this study are summarized in pyroxene quadrilaterals (Fig. 5). In Y-980459, an intermediate composition of the olivine megacrysts is in equilibrium with the composition of the earliest pyroxene (Koizumi et al. 2004; McKay et al. 2004). Crystallization experiments conducted by Koizumi et al. (2004) reproduced the complete pyroxene crystallization trajectories observed in Y-980459. The earliest pyroxenes in the other shergottites (i.e., EETA79001) have Mg# that are potentially in equilibrium with portions of associated olivine megacrysts (i.e., Grover and Orville 1969; Sack 1980; Brown 1980; Beattie 2004). Pyroxene trajectories across the quadrilateral are different among these shergottites. Based on Mg#, the earliest high-Ca clinopyroxene in NWA 1110/1068 may be in equilibrium with late-stage olivine in the megacrysts. In the lherzolitic shergottites, the olivine is too Fe-rich to be in equilibrium with the coexisting pyroxenes. This is probably the result of faster subsolidus reequilibration of Fe-Mg in olivine compared with pyroxene (i.e., McSween and Treiman 1998).

There are significant differences in the zoning profiles between Mg# in Y-980459 and olivine in many of the other shergottites. For example, Y-980459 exhibits a fairly flat profile from core to rim, whereas NWA 2626, EETA79001 and NWA 1110/1068 have fairly homogeneous cores surrounded by rims with significant Fe enrichment (Fig. 6). In addition to this style of zoning, EETA79001 also has olivine with sharp boundaries between homogeneous cores and Fe-rich rims.

In all of the olivine shergottites, MnO increases with decreasing Mg# from olivine core to rim. This behavior is expected based on the predicted behavior of Mn ($D_{Mn}^{ol/basalt}$ = 0.5 to 1.07; Beattie, 1994). Figure 7 also illustrates that there can be substantial overlap in Mg#-MnO in shergottites with significantly different isotopic characteristics (compare Y-980459 to EETA79001 to NWA 1110/1068). This suggests that melts that are parental to these basalts have similar melt compositions with regards to Mg# and Mn.

Whereas, Mn shows a consistent behavior among the olivine-phyric shergottites, Mg#-CaO exhibits a startling contrast (Fig. 8). The olivine in Y-980459 exhibits an increase in CaO with decreasing Mg#. This trajectory probably represents a simple, closed system magmatic signature involving the sole crystallization of olivine. A similar relationship between Mg#-CaO is also observed in olivine from the Makaopuhi lava lake in Hawaii (Hagerty et al. 2006) and Apollo 12 olivine basalts (Papike et al. 1999). In contrast, the olivine from most other shergottites exhibits a near constant CaO with decreasing Mg#. This could reflect the role of pyroxene on the CaO content of the melt during olivine crystallization. In EETA79001 (lithology A), the CaO content consists of two distinct populations. In the olivine cores, CaO increases with near constant Mg#, while in the rims, CaO content overlaps with the core compositions at lower Mg# (Fig. 8). The CaO in olivine from the nakhlites ranges from 0.15 to 0.55 wt.% and appears to reflect oscillatory zoning. The zoning in Fe/Mg in the olivines from the nakhlites reflects continuous diffusive exchange with residual intercumulus magma, whereas the variations in CaO may reflect original growth zoning (Treiman 1990; Harvey and McSween 1992; McSween and Treiman 1998).

Trace Element in Olivine

Ni-Co behave similarly in all Martian olivines analyzed, with Ni decreasing and Co increasing from core to rim (Fig. 9). The cores of Y-980459 and NWA 1110/1068 have the highest Ni abundances. Using core compositions of Y-980459 and bulk Y-980459 compositions, calculated D_s for Ni and Co for these basalts are 7.3–5.5 and 2.4–1.8, respectively. This agrees with experimentally determined D for olivine-melt for these compositions (i.e., $D_{Ni}^{ol/basalt} \approx 6$; melt composition of MgO = 19% and olivine composition of Fo84; Kinzler et al. 1990, whereas $D_{Co}^{ol/basalt}$ = 1.6 to 2.22; Seifert et al. 1988). Surprisingly, most of the Ni-Co zoning trajectories for the olivine overlap except for NWA 1110/1068 and the nakhlites.
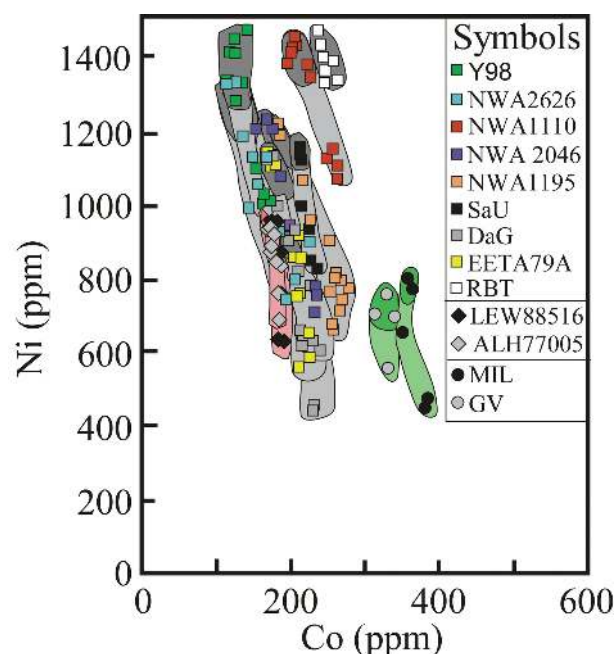

Fig. 9. Plot of Co versus Ni for olivine from the shergottites (gray), lherzolitic shergottites (orange) and nakhlites (green). Cores of olivine are emphasized by slightly darker colors. Symbols are indexed in the figure.

The Ni-Co zoning trajectory in NWA 1110/1068 is parallel to the other olivines but displaced to high Co. The olivine in the nakhlites has lower Ni and higher Co than most of the olivine-bearing shergottites.

Vanadium in Y-980459 (Fig. 10a), A12 olivine basalts, and the Makaopuhi lava lake (Fig. 10b) increases with decreasing Ni from core to rim. This is consistent with the behavior of V in olivine-melt systems where $D_V^{ol/basalt}$ = 0.03 to 0.6 (i.e., Shearer et al. 2006). These three systems represent significantly different fO_2 conditions. The Ni-V slope changes from nearly vertical at terrestrial fO_2 conditions (>FMQ) to a flatter slope at lunar fO_2 conditions (IW-1). Yamato 980459 has an intermediate slope. In contrast to the behavior of V in Y-980459, V in olivine from all the other Martian basalts decreases with decreasing Ni from core to rim.

Shearer et al. (2006) proposed that this behavior may be due to reequilibration between the olivine and melt. Alternatively, differences in V behavior in the olivine shown in Fig. 10 may reflect variations in D_V^{spinel} or the differences in the appearance of spinel and/or pyroxene as liquidus phases that co-crystallize with olivine. Righter et al. (2006b) documented that whereas the D_{Ni}^{spinel} ($\approx$10) and D_{Co}^{spinel} ($\approx$5) are similar to olivine (and are not dramatically dependent on the composition of the early spinel or fO_2), D_V^{spinel} is dependent upon a range of variables (see equation #2 in Righter et al. 2006b). Based on the observations of Righter et al. (2006b), the Ni-Co trajectories as shown in Fig. 9 will not reflect the presents or absence of spinel during olivine crystallization because of the similarity of Co and Ni
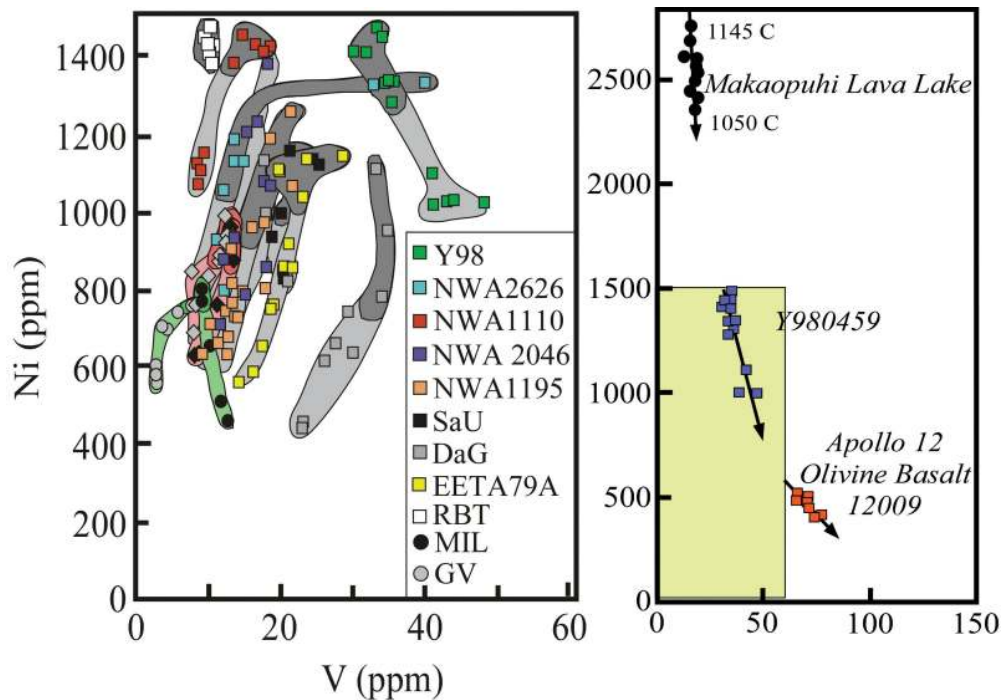
Fig. 10. Plot of V versus Ni for olivine from the shergottites and nahklites. Mg# for bulk rock and olivine is illustrated in Fig. 4.

partitioning behavior for olivine and spinel. In contrast, D_V^{spinel} is substantial higher than $D_V^{olivine}$ and will exhibit considerable variation in magmatic systems. Using Equation 2 from Righter et al. (2006), we were able to approximate D_V^{spinel} for the three systems shown in Fig. 10. The D_V^{spinel} is approximately 14 for the Makaopuhi lava lake, 20 for Martian basalts, and 32 for the A12 olivine basalts. These differences in D_V^{spinel} cannot account for the variations in V that are observed in the olivine in Fig. 10. Goodrich et al. (2003) and McKay et al. (2004) documented the crystallization history of spinel and olivine in many shergottites. They concluded that in most shergottites, spinel co-crystallized with olivine. In Y98, it appears that substantial olivine crystallized prior to the appearance of spinel on the liquidus. Therefore, it appears that differences in V-Ni behavior between Y98 and many of the other shergottites reflect the appearance of spinel on the liquidus.

The relationship between Co/Ni and MnO in olivine and its potential link to fO_2 was first documented by Herd et al. (2000) for a small population of shergottites. In this larger population of Martian basalts, the slope of Co/Ni versus MnO for shergottites lies between the steep slope defined by olivine from the reduced ($fO_2 = IW - 1$) Apollo 12 olivine basalts and the fairly flat slope defined by olivine from the much more oxidizing ($fO_2 \approx FMQ + 0.5$) Makaopuhi lava lake (Hagerty et al. 2006). Most of the Co/Ni and MnO trajectories for the shergottites are parallel to one another. The olivine from NWA 1110/1068 appears to define a somewhat flatter slope (Fig. 11).

NWA 1110/1068 appears to be more enriched in incompatible elements than most of the other olivine-phyric shergottites (Shih et al. 1993; Borg et al. 1997, 2003; Wadhwa 2001; Herd et al. 2002a; Goodrich et al. 2003; Herd 2003, 2006; Jones 2003; Symes et al. 2008). The olivine cores in NWA 1110/1068 have higher Y than olivine from other shergottites (Fig. 12).

Trace Elements in Olivine Melt Inclusions

One of the characteristics differentiating the "enriched" shergottites from the "depleted" shergottites is the shape of the REE pattern for the bulk shergottite (Fig. 1). REE are highly incompatible in olivine and therefore, contrasting REE pattern shape among olivine megacrysts is highly compromised due to the low abundance of REE. To further explore the apparent contrast in the incompatible element characteristics among the shergottites that is reflected in the olivine, we attempted to analyze melt that was trapped as inclusions or embayments in the olivine. These trapped melts may provide some evidence for the composition of the melt from which the olivine crystallized. Our initial analyses of inclusions in the olivine indicate that the REE patterns in NWA 1110/1068 are similar to those determined by Wadhwa and Crozaz (2002) and generally tend to be flat. In Y-980459 our results indicate the melt inclusions generally have a REE pattern that is LREE depleted (Fig. 13). Thus, the REE patterns of the trapped melt in olivine in these two samples are similar to the pattern shapes defined by the bulk rocks.
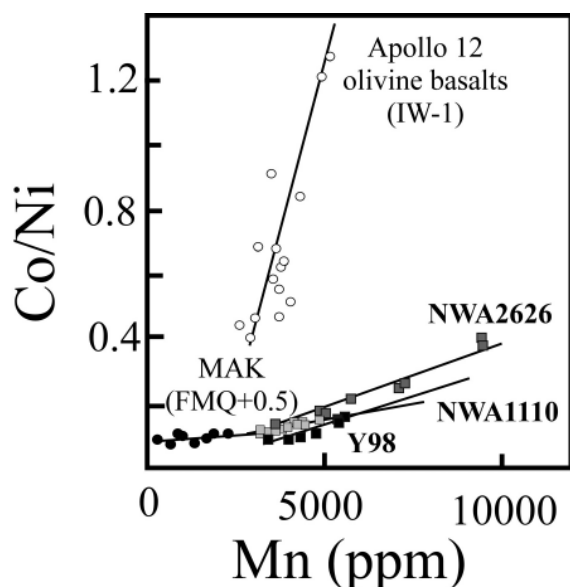
Fig. 11. Plot of MnO versus Co/Ni for olivine from the shergottites, lherzolitic shergottites, and nahklites. Symbols: black circles = MAK, white circles = Apollo 12 olivine basalts, black squares = Y98, dark gray squares = NWA 2626, and light gray squares = NWA 1110.

DISCUSSION

Petrogenesis of Olivine in the Olivine-Bearing Shergottites

The suggested origin for the olivine in the olivine-bearing shergottites includes phenocrystic olivine (McKay et al. 2004; Koizumi et al. 2004; Shearer et al. 2006), minor accumulation of phenocrystic olivine (Shearer et al. 2006), accumulation of megacrystic olivine from the same overall basaltic system (Barrat et al. 2002; Irving et al. 2002, 2005; Wadhwa and Crozaz 2002; Shearer et al. 2006), and xenocrystic olivine that was randomly incorporated into a melt that is basaltic in composition (McSween and Jarosewich 1983; Wadhwa et al. 1994; Treiman 1995; Mittlefehldt et al. 1999; Barrat et al. 2002; Herd et al. 2002b). In the latter case, both magmatic and impact processes have been suggested as mechanisms for olivine incorporation into the melt (McSween and Jarosewich 1983; Wadhwa et al. 1994; Treiman 1995; Mittlefehldt et al. 1999; Herd et al. 2002b). It is probably most likely that all of these processes are relevant to the olivine-bearing Martian basalts to varying degrees. Can we distinguish among them in the current population of olivine-bearing shergottites?

Yamato-980459 is the key for the interpretation of the shergottite olivine data, because textural and chemical attributes of the olivine indicate that it is a phenocryst and in equilibrium or near-equilibrium with the host basaltic melt. The olivine is euhedral and exhibits no indications of absorption in an extraneous magma (Fig. 2). This inference is further reinforced by chemical characteristics of the olivine. The Mg# of the olivine reflects equilibrium with the bulk rock (Fig. 4).
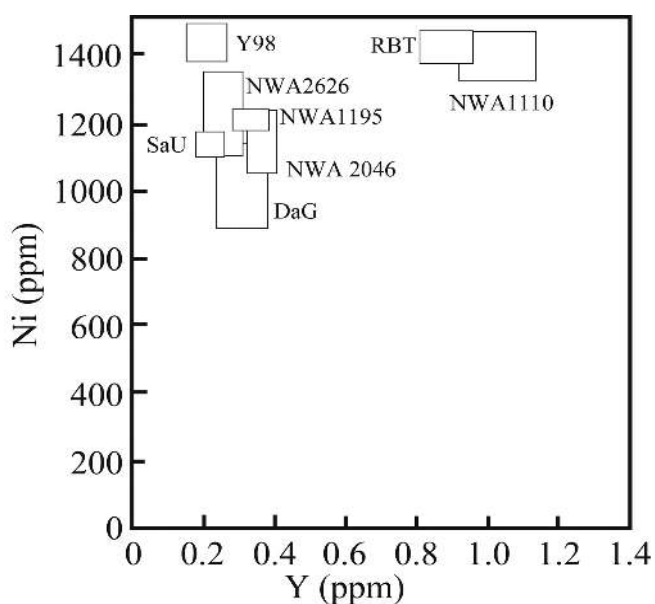

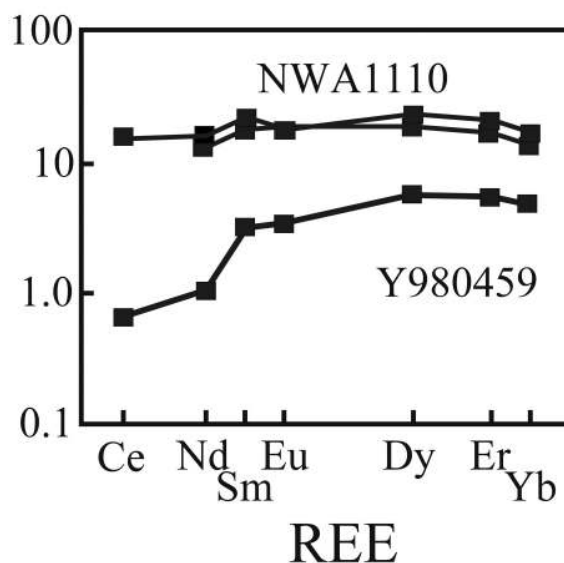Fig. 12. Plot of Y versus Ni for cores of olivine megacrysts.

Fig. 13. REE patterns of melt inclusions within olivine megacrysts from Y-980459 and NWA 1110/1068.

This is similar to olivine-melt relationships in other well documented, closed basalt systems such as the Apollo 12 olivine basalts and early stages of the crystallization of the Makaopuhi lava lake (Fig. 4). Based on the exchange of Fe-Mg between melt, orthopyroxene and olivine (i.e., Grover and Orville 1969; Brown 1980; Sack 1980; Beattie 2004) the first crystallizing pyroxene ($En_{80}Fs_{18}Wo_2$) is of appropriate composition to be in equilibrium with compositions of outer zones in the olivine megacrysts and cores of the smaller olivine in the groundmass (Fo_{80-79}). Crystallization experiments by Koizumi et al. (2004) and McKay et al. (2004) both confirm the petrologic relationship between the first pyroxenes and olivine

megacrysts and reproduced the complete pyroxene crystallization trajectories observed in Y-980459. Further, application of the MELTS algorithm to the crystallization of the Y-980459 bulk composition produced calculated pyroxene compositional trajectories in the pyroxene quadrilateral that reproduce both the experimental and observed pyroxene compositions (Symes et al. 2008). As the texture and mineralogy of Y-980459 implies a relatively simple petrologic relationship between the olivine megacrysts and the surrounding matrix, the behavior of the other major, minor, and trace elements in the olivine megacrysts should reflect crystallization within a closed, relatively simple system. Incompatible elements in olivine such as, Ca ($D^{olivine/basalt} <$ 0.03), Y ($D^{olivine/basalt} < 0.01$), and V ($D^{olivine/basalt} \approx 0.2$ at IW + 1) are inversely correlated to MgO and Mg# and increase from core to rim (Fig. 9 and 11). Highly compatible elements such as Ni decrease with MgO and Mg# from core to rim (Fig. 9), while moderately compatible elements such as MnO ($D^{olivine/basalt} \approx 1.0$) and Co ($D^{olivine/basalt} \approx 2.5$) increase slightly from core to rim (Fig. 8 and 10). An interesting observation that appears to run counter to these mineralogical arguments is that the olivine in Y-980459 lies off the isochron defined by whole rock and pyroxene (Shih et al. 2005). Although this observation could be interpreted as a xenocrystic origin for the olivine, Shih et al. (2005) attributed the isotopic characteristics of the olivine to terrestrial contamination. Similar deviations have been observed in olivine mineral fractions from the lherzolitic shergottites and have also interpreted to reflect contamination (Borg et al. 2002; Edmunson et al. 2005).

In contrast to the olivine in Y-980459, the early olivine in the other shergottites exhibits varying degrees of textural and chemical differences. Based on the Mg# of the early olivine cores relative to the Mg# of the bulk shergottite (Fig. 4), all of the other shergottites appear to have excess olivine. The subhedral to anhedral morphology of many of these olivine megacrysts (Fig. 2) suggests reaction with the host basalt. Further, the zoning characteristics of the megacrystic olivine in these shergottites generally tend to have Fe-rich rims indicative of extensive and perhaps "rapid" reaction between the olivine and the adjacent melt. Although these textures could be interpreted as indicating the incorporation of xenocrystic olivine into an unrelated basalt, comparison with terrestrial basaltic systems indicate that these textures could also be produced during the crystallization of a fairly simple, closed basaltic system. As shown in Fig. 2, samples from the Makaopuhi lava lake contain both euhedral olivine phenocrysts immersed in a basaltic glass (MAK M-18) and "reworked" olivine phenocrysts with Fe-rich rims and absorption textures (MAK M-23-17) similar to that observed in the shergottites. The "reworked" olivine phenocrysts can exist in a basaltic matrix that contains either a small amount of groundmass olivine or no groundmass olivine at all. Observations made during the crystallization of the Makaopuhi lava lake indicate that these textures can be

produced during gravitational settling and convective transport of olivine phenocrysts over a period of time of less than 9 months (Hagerty et al. 2006 and references within). Therefore, textural evidence on its own is ambiguous in establishing either a xenocrystic or phenocrystic origin for the olivine megacrysts in shergottites.

There are several lines of reason that can be followed to argue that the megacrystic olivine in most of the olivine-bearing shergottites is not xenocrystic, but is either a product of olivine accumulation or addition of "cogenetic" olivine. First, Fe-Mg exchange K_D indicates that the earliest pyroxenes are in near equilibrium with olivine compositions preserved within portions of the megacrysts. However, pyroxene compositional trajectories that follow the earliest pyroxenes do deviate from that observed in Y-980459. This could lead to the conclusion that in the case of EETA79001 lithology A, both the olivine and orthopyroxene are xenocrystic. Second, the olivine megacrysts appear to record the co-precipitation of other phases in the surrounding matrix. As an example, based on V and CaO all of the megacrysts (except Y-980459) appear to record the co-precipitation of spinel (decreasing V) and high-Ca pyroxene (constant or decreasing CaO). EETA79001 is somewhat different in that its CaO content defines two distinct populations. Third, the composition of the olivine appears to be closely related to the bulk composition of the bulk rock. For example, melt inclusions in the olivine from Y-980459 and NWA 1110/1068 have REE patterns that mirror the bulk rock (Fig. 13). In addition, olivine in the LREE depleted shergottites have similar characteristics (Ni, Co, Mn zoning trajectories) and appear to have crystallized at similar fO_2, whereas the olivines from the more LREE-enriched shergottites (NWA 1110/1068) have distinctly different characteristics. Again, it is important to note that the olivine in EETA79001 (A) does not appear to fit within this scenario. It has the characteristics of olivine from the LREE-depleted shergottites (Fig. 8 and 10), yet it has a bulk rock isotopic composition and REE abundances that are intermediate between the two shergottite end-members (Fig. 1). Fourth, most of the olivine mineral fractions from basaltic shergottites that have been analyzed for Rb-Sr and/or Sm-Nd appear to be in isotopic equilibrium with plagioclase (maskelynite) and pyroxene. Examples include NWA 1195, Dhofar 019, NWA 1110/1068 (Shih et al. 2003), and DaG 476 (Borg et al. 2001, 2003; Symes et al. 2008). Additional isotopic studies of EETA79001 lithology A may shine additional light on the origin of olivine in this basalt.

Estimates of fO_2 from V Partitioning and the Relationship Between Co/Ni-MnO

Wadhwa (2001), Herd et al. (2002a), Herd (2003), and Goodrich et al. (2003) concluded that the fO_2 in Martian basalts varies by 2 to 4 log units and is correlated with

geochemical parameters such as LREE/HREE, initial $^{87}Sr/^{86}Sr$, and initial ε_{Nd}. As olivine is an early liquidus phase in all of the basalts in this study, the multi-valence partitioning behavior of V between olivine and melt can be used to estimate the early fO_2 crystallization conditions of these basalts (Canil 1997, 1999, 2002; Canil and Fedortchouk 2001; Shearer et al. 2006). Using the behavior of V in olivine in Y-980459, Shearer et al. (2006) estimated that the condition of its initial crystallization was at an fO_2 of IW + 0.9. Both the V^{3+}/V^{4+} of glass in Y-980459 (Sutton et al. 2005; Karner et al. 2006; Shearer et al. 2006) and spinel compositions (McKay et al. 2004) are consistent with an fO_2 of approximately IW + 1. Using the V data from olivine in the other shergottites, Shearer et al. (2006) estimated that the early fO_2 crystallization conditions of NWA 1195 and SaU 005 were similar to Y-980459 at approximately IW + 1, whereas the fO_2 of NWA 1110/1068 was more oxidizing ($\approx$IW + 2). The latter is in contrast to the results of Herd (2006) which estimated fO_2 for the earliest formed olivine to be IW + 1. However, the fO_2 calculations from V partitioning are not as robust as those made for Y-980459 due to some of the assumptions that were made by Shearer et al. (2006). Studies of V partitioning between pyroxene and melt (melt = QUE 94201) indicate that LREE-depleted shergottite QUE 94201 (Fig. 1) crystallized at an fO_2 between IW + 0.5 and IW + 1 (Karner et al. 2007). These data imply that the Martian mantle sources for the LREE-depleted shergottites were at a fO_2 of between IW to IW + 1. Shearer et al. (2006) concluded that the upper mantle of Mars was at an fO_2 of IW to IW + 1, whereas more oxidized reservoirs that contributed to the signature of the LREE-enriched shergottites were either in the Martian crust or deep Martian mantle.

Herd et al. (2001a) observed that the slope of Co/Ni versus MnO in olivine appeared to be linked to the fO_2 under which the basaltic system crystallized. This relationship is illustrated in a comparison of olivine in the Apollo 12 olivine basalts (IW − 1), Makaopuhi lava lake ($\geq$FMQ), and the basaltic shergottites (Fig. 11). The cause of this apparent relationship has not been satisfactorily explained. The experimental study by Herd et al. (Forthcoming) concluded that changes in fO_2 on the scale observed in Martian basalts did not affect the olivine/melt partitioning behavior of Ni or Co; the combined data of Herd et al. (Forthcoming) and Mysen (2006) show that oxygen fugacity influences on Ni and Co partitioning in olivine are only significant above ~IW + 3. In almost all olivine in Martian basalts, little Fe-Mg subsolidus re-equilibration has occurred; since diffusion rates in olivine are generally Fe ~ Mg > Co > Ni (Ito et al. 1999) the changes in slope cannot be attributed to differences in the degree of subsolidus reequilibration and differences in diffusivities of Ni, Co, and Mn. Extensive studies by Righter et al. (2006a, b) indicate that DNi and DCo in spinel are not affected by fO_2. Based solely on this observation, it would appear that spinel co-crystallizing with olivine should not affect olivine zoning. However, this is still a point of contention. McKay et al. (2004) illustrated that for Martian basalt compositions, the composition of spinel and the point at which it appears on the liquidus is controlled by fO_2. Both of these variables could influence the behavior of Ni and Co in spinel. Both manifestations of changing fO_2 could potentially affect the Co/Ni zoning observed in the olivine.

Our new data for additional shergottites generally fit the initial observations of Herd et al. (2001a). The relatively oxidized NWA 1110/1068 has a shallow slope on a plot of Ni-Co, with the more reduced Y-980459, NWA 2046 and NWA 1195 having steeper slopes (Fig. 11). Taken at face value, the Co/Ni-Mn slopes indicate that the highly depleted olivine-bearing shergottites started crystallizing at similar fO_2, whereas NWA 1110/1068 crystallized at more oxidizing conditions.

Petrogenetic Relationships Among the Olivine-Bearing Shergottites

The olivine-bearing shergottites represent Martian basaltic magmatism that occurred over a time span of at least 410 million years from 170 to 580 Ma (Table 1). Incompatible elements and incompatible element-based isotopic systems indicate that they are crystallization products of basaltic melts produced through the mixing of at least two end-member reservoirs (Fig. 1). Based upon isotopic systematics, the olivine-bearing shergottites such as Y-980459, NWA 1195, Dhofar 019, and DaG 476 are derived from the LREE-depleted source. Our olivine data suggests that NWA 2626, NWA 2046, and SaU 005 also fit within this group. Only EETA79001 lithology A and NWA 1110/1068 have isotopic and geochemical signatures that are representative of the involvement of the enriched end-member reservoir (Fig. 1). Thus far, no radiogenic isotopic measurements have been produced for RBT 04261.

In addition to the incompatible element signatures documented for the depleted olivine-bearing shergottites, their olivine megacrysts crystallized from magmas with other similar characteristics. First, they all crystallized at an fO_2 of between IW and IW + 1 indicating that they were derived from reduced (IW to IW + 1) and LREE-depleted mantle sources. The olivine data indicate that many of the primary melts from which these basalts were derived had similar Ni, Co, and Mn abundances. Analyses of olivine indicate that these primary melts may have exhibited more deviation in Cr and V, although the observed deviations may also be a product of the effect of early spinel crystallization on the abundances in the melt at the time olivine crystallized. Therefore, we conclude that the parental magmas of the LREE-depleted suite of olivine-bearing shergottites were derived from similar sources in the upper mantle.

Only one of the highly LREE-depleted basalts does not have olivine on the liquidus: QUE 94201. Nevertheless, this basalt has similar initial isotopic Sr and Nd isotopic

compositions, and incompatible element characteristics (Fig. 1). The calculated fO_2 for the crystallization of QUE 94201 that is based on Eu valence state partitioning ranges from IW − 1.5 and IW + 1 (Wadhwa 2001; Musselwhite and Jones 2003; McCanta et al. 2004), However, based on V and Cr partitioning between early pigeonite and the QUE 94201 melt composition, Karner et al. (2007) estimated that QUE 94201 crystallized under an fO_2 of between IW + 0.2 and IW + 0.9 and thus under fO_2 conditions that are very similar to the other LREE-depleted shergottite group. This is consistent with the estimate of Herd et al. (2001b) based on Fe-Ti oxide oxybarometry (IW + 0.5 to IW + 1.6). Given these observations, it appears likely that QUE 94201 was a product of fractional crystallization of parental basalt with characteristics similar, but not identical to, Y-980459. This conclusion is supported by modeling by Symes et al. (2007) that illustrated that ~45% crystallization of a Y-980459 composition would yield an evolved basaltic melt that had many on the mineralogical and chemical characteristics of QUE 94201.

Based on isotopic and trace element characteristics (both bulk rock and in olivine), only olivine-bearing shergottites NWA 1110/1068, EETA79001 lithology A and RBT 04261 appear to have signatures representative of an "enriched" component (Fig. 1). NWA 1110/1068 has the most LREE-enriched signature and is similar in this regard to Los Angeles, Shergotty, Zagami, and NWA 856. RBT 04261 has olivine megacrysts with trace element characteristics as NWA 1110/1068. Conversely, EETA79001 (lithology A) has REE systematics and isotopic systematics that are intermediate between the LREE-depleted and LREE-enriched groups (e.g., Symes et al. 2008) It is therefore similar to EETA79001 (B), NWA 1460, and the lherzolitic shergottites such as ALH 77005 and LEW 88516. There are several models for the relationship among the "depleted" and "enriched" shergottites: (Model 1) The array defined by the shergottites (i.e., Fig. 1) represents mixing of two mantle components (enriched-oxidized source versus depleted-reduced source) prior to melting. The characteristics of the resulting magmas are an intrinsic property of the sources. (Model 2) The basalts are primarily produced through polybaric melting of large proportions of a reduced LREE depleted source, combined with a variable, and volumetrically minor proportion, of an oxidized LREE-enriched source. Thus, the LREE-enriched and oxidized mantle assemblage could be added to the initial basaltic melt as rises though the mantle (e.g., Borg et al. 1997; 2003; Borg and Draper 2003; Symes et al. 2008). Clearly, the "enriched" mantle component in both of these petrogenetic models may represent the last stages of a Martian magma ocean (MMO). (Model 3) Shergottitic basalts are primarily produced through the melting of "depleted" and reduced sources. These basalts assimilated an "enriched"-oxidized assemblage that resides in the Martian crust. The "enriched" crustal component was produced during the early

differentiation of Mars and has been modified by fluids (oxidation of assemblage, exchange of stable isotopes) over the last 4 billion years.

The olivine in EETA79001 (lithology A) is not distinctly different from the olivine in the "depleted shergottites"; oxybarometry of the megacryst assemblage yields IW + 1 (Herd 2003), olivine is similar to the incompatible element depleted shergottites discussed above. This lack of difference could be interpreted as indicating either the olivine is xenocrystic within an "enriched" and more oxidized basalt (the groundmass of EET7 9001 lithology A gives IW + 2, both from ol-px-sp and Fe-Ti oxides) or that the small mass of "enriched" component required to be mixed into this basalt does not dramatically influence many of the elements incorporated into olivine. The record preserved in the olivine in NWA 1110/1068 is clearly different and does provide some key insights into the mechanisms by which the enriched component is incorporated into these basalts. The olivine in NWA 1110/1068 is more enriched in Co and incompatible elements such as Y, and crystallized from a basaltic melt that had a flat REE pattern. These data indicate that this enriched component was added to the melt prior to olivine crystallization. This could indicate that this enriched component is an intrinsic characteristic of the primary melt and consequently located in the mantle source region. Alternatively, this component could have been added through assimilation of the Martian crust. In this case, the olivine in NWA 1110/1068 does not record the geochemistry of the mantle derived melt because it crystallized after assimilation. The early olivine that would have been characterized by low Y and LREE-depleted REE patterns was efficiently removed during assimilation and prior to eruption

Although NWA 1110/1068 is enriched in incompatible elements relative to Y98, the olivine from these two meteorites crystallized from basaltic melts with similar Ni abundances (the whole rock (melt) Ni content of Y98 is approximately 270 ppm). High pressure studies of Y98 have been interpreted to indicate that its bulk composition was derived through melting at Martian mantle conditions (Burgess et al. 2006; Draper 2007). If the olivine in Y98 and NWA 1110/1068 records the composition of near-primary Martian basalts, the Ni content of their sources is similar. Within the context of MMO models suggested for shergottite mantle sources (Herd et al. 2002a; Borg and Draper 2003; Borg et al. 2003; Herd 2003; Symes et al. 2008), the mantle source for the NWA 1110/1068 basalt could not simply be a late-stage MMO cumulate, but a source dominated by early-(depleted) MMO cumulates with a very small proportion of late- (enriched) stage MMO cumulates. This stems from the fact that the incorporation of large proportions of late-(enriched) stage MMO cumulates would dramatically lower the Ni content of the parental melts from which the NWA 1110/1068 olivines crystallized.

These data also constrain possible crustal assimilation

models for the shergottites. For the addition of the enriched component to be a product of crustal assimilation, the Ni content and Mg# of the parental basalt to NWA 1110/1068 must have been significantly higher prior to assimilation. Assimilation and fractional crystallization would have resulted in olivine crystallization and a decrease in Ni. For example, if assimilation was accompanied by only 10% olivine crystallization, the Ni content of the parental melt to NWA 1110/1068 must have been approximately 510 ppm. Thus far, no Martian basalt with 500 ppm Ni has been identified, although the olivine in RBT04261 (high Ni and relatively low Mg#) suggests such basalts exist.

The partitioning of vanadium between olivine and melt suggests that the early olivine in NWA 1110/1068 crystallized at a more oxidizing fO_2 (>IW + 2) than the other olivine-bearing shergottites. This contrasts with the interpretation of textural and mineralogical observations (Herd 2003) that appear to indicate that the early olivine crystallized at more reducing conditions ($\approx$IW + 1) and then experienced oxidation during crystallization (>IW + 2). If the observation of Herd (2003) is correct, it suggests that the incorporation of the "enriched" signature is decoupled from the oxidation. This would indicate that the "enriched" component in NWA 1110/1068 is at conditions of IW to IW + 1. This suggests that the isotopic-signatures of all shergottites with LREE-enriched elemental and isotopic characteristics that crystallized under relatively oxidized conditions were produced in a similar manner (Wadhwa et al. 2001; Herd et al. 2002a; Herd 2003).

Relevance of the Olivine Data to Interpreting the Martian Surface as Determined by Mars Exploration Rover Mission (MER)

The Alpha Particle X-ray Spectrometer (APXS) on the MER was used to determine the Ni content of Martian soils. The Ni content of the Algonquin class rocks (Fig. 14) (except for Larry's Bench) are much greater than that of Gusev plains basalt (Dreibus et al. 2006) or many of the olivine-bearing Martian meteorites. The enrichments of the Gusev soil in Ni were explained by a meteoritic component that was admixed by impacts (Dreibus et al. 2006; Yen et al. 2005). The identification of Fe-Ni meteorites on the surface of Mars further supported the addition of a meteorite contribution to the Martian soil. Yen et al. (2005) estimated this contribution to be between 1 and 3%.

There is another Ni-bearing component that will lower the calculated abundance of the meteorite component in the Martian soil. As illustrated in Fig. 14, the olivine megacrysts in the olivine-bearing shergottites plot near the intersection between the Algonquin class line and 100% olivine. Orbital observations (i.e., Hoefen et al. 2003) suggest olivine is abundant on the Martian surface and may not have experienced significant recent alteration. These two lines of observations suggest the possibility that the olivine from Martian basalts
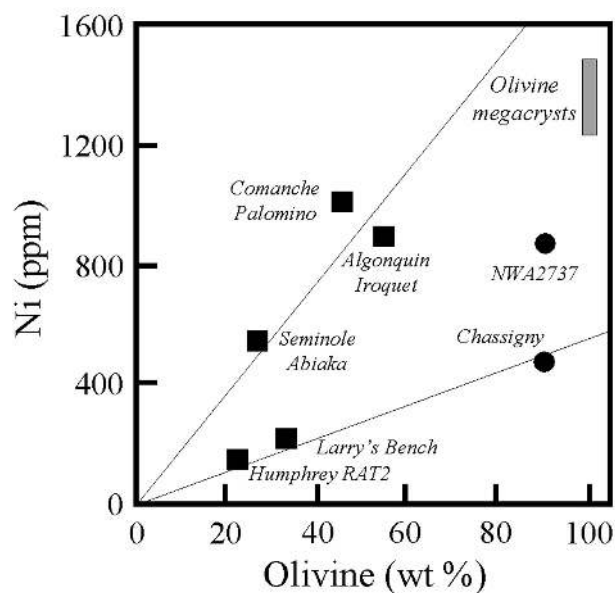

Fig. 14. Plot of estimated olivine versus Ni abundance for Gusev rocks, Chassigny, and NWA 2737 (after Dreibus et al. 2007). Olivine megacrysts plot near the end of the "Algonquin high-Ni trend."

may have been separated from the basalts through the alteration of fine-grained mesostasis and incorporated into the soil. If correct, estimates of meteorite contributions to the Martian soil should be recalculated. This may have profound implications for calculations of both the present day meteorite flux of Mars and the overall age of the Martian soil.

CONCLUSIONS

The olivine in shergottites generally tends to reflect the overall character of the basalt in which they occur (enriched/depleted, fO_2). In the case of NWA 1110/1068, this implies that the "enriched component" was added to system prior to olivine crystallization as the chemical characteristics of the olivine and melt inclusions trapped in the olivine have an "enriched signature". In addition, this observation implies that in most cases the olivine was not randomly incorporated into the basalt, but is co-genetic in some manner. This co-genetic relationship may be as simple as the accumulation of phenocrysts at the base of a flow or reflect more complex behavior such as mixing of olivine phenocrysts into a co-genetic basalt. This could be similar to processes that were active in the Makaupuhi lava lake. EETA79001 appears to be distinct from the other olivine-bearing shergottites with regards to the olivine characteristics and relationship between the olivine and surrounding matrix.

The V data indicates a limited range of fO_2 of crystallization for the "depleted" olivine-bearing shergottites (~IW to IW + 1). This probably reflects the fO_2 conditions of the Martian upper mantle. It has been suggested that the reservoir that represents the "enriched" end-member in the

shergottites suite could be more oxidized (>IW + 2) and reside in the lower Martian crust or lower mantle. The LREE enrichment appears to be a feature of the basalt prior to olivine crystallization. Herd (2006) concluded that basalts represented by NWA 1110/1068 experienced more oxidizing conditions following olivine crystallization. This seems to suggest the occurrence of two decoupled processes, and somewhat incongruent with strict correlations between mineralogical and geochemical indices of oxidation-reduction and LREE depletion-enrichment.

The significant overlap in olivine compositions in many of the "depleted" olivine-bearing shergottites may be interpreted as indicating that they crystallized from basalts with many similar characteristics. Therefore, it appears that the Martian mantle is capable of producing melts of similar composition over a time period of at least 0.5 billion years.

Differences in olivine megacrysts in shergottites relative to Y-980459 reflect the response of olivine to the co-precipitation of other phases (spinel, pyroxene) and late-stage reequilibration with an evolving melt. Differences in the extent of late-stage reequilibration of the olivine may be partially tied to cooling rate, crystallization kinetics or in the case of EETA79001 lithology A incorporation into a distinctly different basaltic melt. Future detailed radiogenic isotopic analyses of EETA79001 lithology A will confirm if the olivine in these lithologies are not in isotopic equilibrium with the surrounding basaltic matrix as our observations suggest. Alternatively, we would have to reinterpret our data if the olivine is in isotopic equilibrium with the adjacent basaltic melt.

Melts from which the olivine-phyric shergottites were derived are parental to both "depleted" and "enriched" shergottites. For example, Symes et al. (2007) demonstrated that basalts with a composition similar to Y-980459 would be capable of producing basalts similar in composition to more evolved, LREE-depleted basalts such as QUE 94201. In the same manner, the basaltic melt that produced NWA 1110/1068 has a composition that is similar to melts parental to Shergotty, Los Angeles and Zagami.

The relatively high Ni in the olivine from the shergottites and the potential for olivine contributing to the Ni content of the Martian soils has implications for recent Martian surficial processes, current impact flux, and the age of the Martian soil.

REFERENCES

Barrat J. A., Jambon A., Bohn M., Gillet. Ph, Sautter V., Göpel C., Leisured M., and Keller F. 2002. Petrology and chemistry of the picritic shergottite North West Africa 1068 (NWA 1068). *Geochimica et Cosmochimica Acta* 66:3505–3518.

Beattie P. 1994. Systematics and energetics of trace-element partitioning between olivine and silicate melts: Implications for the nature of mineral/melt partitioning. *Chemical Geology* 117: 57–71.

Beattie P. 2004. Olivine-melt and orthopyroxene-melt equilibria. *Contributions to Mineralogy and Petrology* 115:103–111.

Blichert-Toft J., Gleason J. D., Télock P., and Albarède F. 1999. The Lu-Hf isotope geochemistry of shergottites and the evolution of the Martian mantle-crust system. *Earth and Planetary Science Letters* 173:25–39.

Borg L. E., Nyquist L. E., Taylor L. A., Wiesmann H., and Shih C. Y. 1997. Constraints on Martian differentiation processes from Rb-Sr and Sm-Nd isotopic analyses of the basaltic shergottite QUE 94201. *Geochimica et Cosmochimica Acta* 61:4915–4931.

Borg L. E., Nyquist L. E., Wiesmann H., and Reese Y. 2002. Constraints on the petrogenesis of Martian meteorites from Rb-Sr and Sm-Nd isotopic systematics of the lherzolitic shergottites ALH 77005 and LEW 88516. *Geochimica et Cosmochimica Acta* 66:2037–2053.

Borg L. E., Nyquist L. E., Wiesmann H., Shih C. Y., and Reese Y. 2003. The age of Dar al Gani 476 and the differentiation history of the Martian meteorites inferred from their radiogenic isotopic systematics. *Geochimica et Cosmochimica Acta* 67:3519–3536.

Borg L. E. and Drake M. J. 2005. A review of meteorite evidence for the timing of magmatism and of surface or near-surface liquid water on Mars. *Journal of Geophysical Research* 110,E12SO3, doi:10.1029/2005JE002402.

Borg L. E., Nyquist L. E., Reese Y., Wiesmann H., Shih C. Y., Ivanova M., Nazarov M. A., and Taylor L. A. 2001. The age of Dhofar 019 and its relationship to the other Martian meteorites (abstract #1144). 32nd Lunar and Planetary Science Conference. CD-ROM.

Borg L. E., and Draper D. S. 2003. A petrogenetic model for the origin and compositional variation of the Martian basaltic meteorites. *Meteoritics & Planetary Science* 38:1713–1731.

Brandon A. D. and Draper D. S. 1996. Constraints on the origin of the oxidation state of mantle overlying subduction zones: An example from Simoe, Washington, USA. *Geochimica et Cosmochimica Acta* 60:1739–1749.

Brown G. E. 1980. *Olivines and silicate spinels*. In *Orthosilicates*, edited by Ribbe P. H. Reviews in Mineralogy, vol. 5. Washington D.C.: Mineralogical Society of America. pp. 275–381.

Burgess K. D., Musselwhite D. S., and Treiman A. H. 2006. Experimental petrology of olivine-phyric shergottite NWA 1068: Toward defining a parental melt (abstract #1972). 37th Lunar and Planetary Science Conference. CD-ROM.

Candela P. A. 1986. The evolution of aqueous vapor from silicate melts: Effect on oxygen fugacity. *Geochimica et Cosmochimica Acta* 50:1205–1211.

Canil D. 1997. Vanadium partitioning and the oxidation state of Archaean komatiite magmas. *Nature* 389:842–845.

Canil D. 1999. Vanadium partitioning between orthopyroxene, spinel, and silicate melt and the redox states of mantle source regions for primary magmas. *Geochimica et Cosmochimica Acta* 63:557–572.

Canil D. 2002. Vanadium in peridotites, mantle redox and tectonic environments: Archean to present. *Earth and Planetary Science Letters* 195:75–90.

Canil D. and Fedortchouk Y. 2001. Olivine-liquid partitioning for vanadium and other trace elements with applications to modern and ancient picrites. *Canadian Mineralogist* 39:319–330.

Draper D. S. 2007. Water-undersaturated near-liquidus phase relations of Y-980459: Preliminary results (abstract #1447). 38th Lunar and Planetary Science Conference. CD-ROM.

Dreibus G., Bruckner J., Gellert R., Jagoutz E. Klingelhofer G., Schmidt M. E., and the Athena Science Team. 2006. Algonquin class rocks of the Columbia Hills in the Gusev crater, Mars, and their relationship to SNC meteorites (abstract #1649). 38th Lunar and Planetary Science Conference. CD-ROM.

Edmunson J., Borg L. E., Shearer C. K., and Papike J. J. 2005. Defining the mechanisms that disturb the Sm-Nd isotopic systematics of Martian meteorites: Examples from Dar al Gani 476 and Allan Hills 77005. *Meteoritics & Planetary Science* 40:1159–1174.

Frost B. R. and Ballhaus C. 1998. Comments on "Constraints on the origin of the oxidation state of mantle overlying subduction zones: An example from Simoe, Washington, USA. *Geochimica et Cosmochimica Acta* 62:329–331.

Goodrich C. A., Herd C. D. K., and Taylor L. A. 2003. Spinels and oxygen fugacity in olivine-phyric and lherzolitic shergottites. *Meteoritics & Planetary Science* 38:1773–1792.

Grover J. E. and Orville P. M. 1969. The partitioning of cations between coexisting single- and multi-site phases with application to the assemblages: Orthopyroxene-clinopyroxene and orthopyroxene-olivine. *Geochimica et Cosmochimica Acta* 33:205–226.

Hagerty J. J., Shearer C. K., Vaniman D. T., and Burger P. V. 2006. Identifying the effects of petrologic processes in a closed system using trace element concentrations in olivine and glasses: Implications for comparative planetology. *American Mineralogist* 91:1499–1508.

Harvey R. P., Wadhwa M., McSween H. Y. Jr., and Crozaz G. 1993. Petrology, mineral chemistry, and petrogenesis of Antarctic shergottite LEW 88516. *Geochimica et Cosmochimica Acta* 57:4769–4783.

Harvey R. P. and McSween H. Y. Jr. 1992. Parent magma of the nakhlite meteorites: Clues from melt inclusions. *Earth and Planetary Science Letters* 111:467–482.

Herd C. D. K. 2003. The oxygen fugacity of olivine-phyric Martian basalts and the components within the mantle and crust of Mars. *Meteoritics & Planetary Science* 38:1793–1805.

Herd C. D. K. 2006. Insights into the redox history of the NWA 1068/1110 Martian basalt from mineral equilibria and vanadium oxybarometry. *American Mineralogist* 91:1616–1627.

Herd C. D. K., Jones J. H., Shearer C. K., and Papike J. J. 2001a. Systematics of Ni, Co, Cr, and V in olivine from planetary melt systems: Martian basalts (abstract #1635). 32nd Lunar and Planetary Science Conference. CD-ROM.

Herd C. D. K., Papike J. J., and Brearley A. J. 2001b. Oxygen fugacity of the Martian basalts from electron microprobe oxygen and TEM-EELS analyses of Fe-Ti oxides. *American Mineralogist* 86:1015–1024.

Herd C. D. K., Borg L. E., Jones J. H., and Papike J. J. 2002a. Oxygen fugacity and geochemical variations in the Martian basalts: Implications for Martian basalt petrogenesis and the oxidation state of the upper mantle of Mars. *Geochimica et Cosmochimica Acta* 66:2025–2036.

Herd C. D. K., Schwandt C. S., Jones J. H., and Papike J. J. 2002b. An experimental and petrographic investigation of Elephant Moraine 79001 lithology: Implications for its petrogenesis and the partitioning of chromium and vanadium in a Martian basalt. *Meteoritics & Planetary Science* 37:987–1000.

Herd C. D. K., Shearer C. K., and Dwarzski R. E. Forthcoming. Experimental investigation of the behavior of Co in olivine in planetary basalts. *American Mineralogist*.

Hoefen T. M., Clark R. N., Bandfield J. L., Smith M. D., Pearl J. C., and Christensen P. R. 2003. Discovery of olivine in the Nili Fossae region of Mars. *Science* 302:627–630.

Irving A. J., Kuehner S. M., Hupe A. C., and Hupe G. M. 2002. Olivine-phyric basaltic shergottite NWA 1195: A very primitive Martian lava (abstract). *Meteoritics & Planetary Science* 37:A69.

Irving A. J., Bunch T. E., Wittke J. H., and Kuehner S. M. 2005. Olivine-orthopyroxene-phyric shergottites NWA 2626 and DaG 476: The Tharsis connection (abstract #1229). 36th Lunar and Planetary Science Conference. CD-ROM.

Ito M., Yurimoto H., Morioka M., and Nagasawa H. 1999. Co^{2+} and Ni^{2+} diffusion in olivine determined by secondary ion mass spectrometry. *Physics and Chemistry of Minerals* 26:425–431.

Jones J. H. 1989. Isotopic relationships among the shergottites, the nakhlites, and Chassigny. Proceedings 19th Lunar and Planetary Science Conference. pp. 465–474.

Jones J. H. 2003. Constraints on the structure of the Martian interior determined from the chemical and isotopic systematics of SNC meteorites. *Meteoritics & Planetary Science* 38:1807–1814.

Karner J. M., Sutton S. R., Papike J. J., Shearer C. K., Jones J. J., and Newville M. 2006. Application of a new V valence oxybarometer to basaltic glasses from the Earth, Moon, and Mars. *American Mineral*ogist 91:270–277.

Karner J. M., Papike J. J., Shearer C. K., McKay G., Le L., and Burger P. 2007. Valence state partitioning of Cr and V between pyroxene melt. Estimates of oxygen fugacity for Martian basalt QUE 94201. *American Mineralogist* 92:1238–1241.

Kinzler R. J., Grove T. L., and Recca S. I. 1990. An experimental study on the effect of temperature and melt composition on the partitioning of nickel between olivine and silicate melt. *Geochimica et Cosmochimica Acta* 54:1255–1265.

Koizumi E., Mikouchi T., McKay G., Monkawa A., Chokai J., and Miyamoto M. 2004. Yamato-980459: Crystallization of Martian magnesian magma (abstract #1494). 35th Lunar and Planetary Science Conference. CD-ROM.

McCanta M. C., Rutherford M. J., and Jones J. H. 2004. An experimental study of rare earth element partitioning between a shergottite melt and pigeonite: Implications for the oxygen fugacity of the Martian interior. *Geochimica et Cosmochimica Acta* 68:1943–1952.

McKay G., Le L., Schwandt C., Mikouchi T., Koizumi E., and Jones J. 2004. Yamato-980459: The most primitive shergottite (abstract #2154). 35th Lunar and Planetary Science Conference. CD-ROM.

McSween H. Y. Jr. and Jarosewich E. 1983. Petrogenesis of the EETA79001 meteorite: Multiple magma pulses on the shergottite parent body. *Geochimica et Cosmochimica Acta* 47:1501–1513.

McSween H. Y. Jr. and Treiman A. H. 1998. Martian samples. In *Planetary materials,* edited by Papike J. J. Reviews in Mineralogy, vol. 36. Chapter 4. Washington, D.C.: Mineralogical Society of America.

Meyer C. 2007. Mars Meteorite Compendium. http://curator.jsc.nasa.gov/ antmet/mmc/mmc.htm.

Mittlefehldt D. W., Lindström D. J., Lindström M. M., and Martinez R. R. 1999. An impact–melt origin for lithology A of Martian meteorite Elephant Moraine A79001. *Meteoritics & Planetary Science* 34:357–367.

Musselwhite D. S. and Jones J. H. 2003. Oxygen fugacity of the Martian mantle from pyroxene/melt partitioning of REE (abstract #2032). 34th Lunar and Planetary Science Conference. CD-ROM.

Mysen B. O. 2006. Redox equilibria of iron and silicate melt structure: Implications for olivine/melt element partitioning. *Geochimica et Cosmochimica Acta* 70:3121–3138.

Papike J. J., Ryder G., and Shearer C. K. 1998. Lunar samples. In *Planetary materials*, edited by Papike J. J. Reviews in Mineralogy, vol. 36. pp. 5-1–5-234.

Papike J. J., Fowler G. W., Adcock C. T., and Shearer C. K. 1999. Systematics of Ni and Co in olivine from planetary melt systems: Lunar mare basalts. *American Mineralogist* 84:392–399.

Papike J. J., Karner J. M., and Shearer C. K. 2005. Comparative planetary mineralogy: Valence state partitioning of Cr, Fe, Ti, and V among crystallographic sites in olivine, pyroxene, and spinel from planetary basalts. *American Mineralogist* 90:277–290.

Righter K., Sutton S. R., Newville M., Le L., Schwandt C. S., Uchida H., Lavina B., and Downs R. T. 2006a. An experimental study of the oxidation state of vanadium in spinel and basaltic melt with implications for the origin of planetary basalts. *American Mineralogist* 91:1643–1656.

Righter K., Leeman W. P., and Hervig R. L. 2006b. Partitioning of Ni, Co, and V between spinel-structured oxides and silicate melts: Importance of spinel composition. *Chemical Geology* 227:1–25.

Roeder P. L. and Emslie R. F. 1970. Olivine-liquid equilibrium. *Contributions to Mineralogy and Petrology* 29:275–289.

Sack R. O. 1980. Some constraints on the thermodynamic mixing properties of Fe-Mg orthopyroxenes and olivines. *Contributions to Mineralogy and Petrology* 71:257–269.

Sato M. and Wright T. L. 1966. Oxygen fugacities directly measured in magmatic gases. *Science* 153:1103–1105.

Seifert S., O'Neill H. S., and Brey G. 1988. The partitioning of Fe, Ni, and Co between olivine, metal, and basaltic liquid—An experimental and thermodynamic investigation, with application to the composition of the lunar core. *Geochimica et Cosmochimica Acta* 52:603–616.

Shannon R. D. and Prewitt C. 1969. Effective ionic radii in oxides and fluorides. *Acta Crystallographica B* 25:925–946.

Shearer C. K. and Papike J. J. 2005. Early crustal building processes on the Moon: Models for the petrogenesis of the magnesian suite. *Geochimica et Cosmochimica Acta* 69:3445–3461.

Shearer C. K., Papike J. J., and Karner J. 2005. Eu valence oxybarometer in pyroxenes. effects of pyroxene composition-crystallization kinetics and comparison between lunar basalts and eucrites (abstract). Workshop on the Oxygen in the Solar System.

Shearer C. K., Papike J. J., and Karner J. M. 2006. Pyroxene europium valence oxybarometer. effects of pyroxene composition, melt composition, and crystallization kinetics. *American Mineralogist* 91:1565–1573.

Shih C. Y., Nyquist L. E., Bogard D. D., McKay G. A., Wooden J. L., Bansal B. M., and Wiesmann H. 1982. Chronology and petrogenesis of young achondrites, Shergotty, Zagami, and ALHA77005: Late magmatism on a geologically active planet. *Geochimica et Cosmochimica Acta* 46:2323–2344.

Shih C. Y., Nyquist L. E., Wiesmann H., and Barrat J. A. 2003. Age and petrogenesis of picritic shergottite NWA 1068: Sm-Nd and Rb-Sr isotopic studies (abstract #1439). 34th Lunar and Planetary Science Conference. CD-ROM.

Shih C. Y., Nyquist L. E., Wiesmann H., Reese Y. and Misawa K., 2005. Rb-Sr and Sm-Nd dating of olivine-phyric shergottite Yamato-980459; Petrogenesis of depleted shergottites. *Antarctic Meteorite Research* 18:46–65.

Shirai N. and Ebihara M. 2004. Chemical characteristics of Martian meteorite, Yamato-980459. *Antarctic Meteorite Research* 17:55–67.

Sutton S. R., Karner J. M., Papike J. J., Delaney J. S., Shearer C. K., Newville M., Eng P., Rivers M., and Dyar M. D. 2005. Vanadium K edge XANES of Synthetic and natural basaltic glasses and application to microscale oxygen barometry. *Geochimica et Cosmochimica Acta* 69:2333–2348.

Symes S. J., Borg L. E., Shearer C. K., and Irving A. J. 2008. The age of the Martian meteorite Northwest Africa 1195 and the differentiation history of the shergottites. *Geochimica et Cosmochimica Acta* 72:1696–1710.

Treiman A. H. 1990. Complex petrogenesis of the Nakhla (SNC) meteorite: Evidence from petrography and mineral chemistry. Proceedings, 20th Lunar and Planetary Science Conference. pp. 273–280.

Treiman A. H. 1995. SNC: Multiple source areas for Martian meteorites. *Journal of Geophysical Research* 100:5329–5340.

Wadhwa M. 2001. Redox state of Mars' upper mantle and crust from Eu anomalies in shergottite pyroxene. *Science* 292: 1527–1530.

Wadhwa M. and Crozaz G. 1994. Trace element abundances in minerals of two new and distinct basaltic shergottites NWA 856 and NWA 1068. *Meteoritics & Planetary Science* 37:A145.

Wadhwa M., McSween Jr., H. Y., and Crozaz G. 1994. Petrogenesis of shergottite meteorites inferred from minor and trace element microdistributions. *Geochimica et Cosmochimica Acta* 58:4213–4229.

Wooden J. L., Shih C. Y., Nyquist L. E., Bansal B. M., Wiesmann H., and McKay G. A. 1982. Rb-Sr and Sm-Nd isotopic constraints on the origin of EETA79001: A second Antarctic shergottite (abstract). 13th Lunar and Planetary Science Conference. pp. 879–880.

Wright T. L. and Okamura R. T. 1977. Cooling and crystallization of tholeiitic basalt, 1965 Makaopuhi Lava Lake, Hawaii. Geological Survey Professional Paper #1004. p.78.

Yen A., Gellert R., Schröder C., Morris R. V., Bell J. F., III, Knudson A. T., Clark B. C., Ming D. W., Crisp J. A., Arvidson R. E., Blaney D., Brückner J., Christensen P. R., DesMarais D. J., de Souza P. A. Jr., Economou T. E., Ghosh A., Hahn B. C., Herkenhoff K. E., Haskin L. A., Hurowitz J. A., Jolliff B. L., Johnson J. R., Klingelhöfer G., Madsen M. B., McLennan S. M., McSween H. Y., Richter L., Rieder R., Rodionov D., Soderblom L., Squyres S. W., Tosca N. J., Wang A., Wyatt M., and Zipfel J. 2005. An integrated view of the chemistry and mineralogy of Martian soils. *Nature* 436:49–54.